Beyond Diagonal RIS-Aided Networks: Performance Analysis and Sectorization Tradeoff

Mostafa Samy, *Student Member, IEEE*, Hayder Al-Hraishawi, *Senior Member, IEEE*, Abuzar B. M. Adam, *Member, IEEE*, Symeon Chatzinotas, *Fellow, IEEE*, and Björn Otteresten, *Fellow, IEEE*

***Abstract*—Reconfigurable intelligent surfaces (RISs) have emerged as a spectrum- and energy-efficient technology to enhance the coverage of wireless communications within the upcoming 6G networks. Recently, novel extensions of this technology, referred to as multi-sector beyond diagonal RIS (BD-RIS), have been proposed, where the configurable elements are divided into L sectors $(L \geq 2)$ and arranged as a polygon prism, with each sector covering $1/L$ space. This paper presents a performance analysis of a communication system that is assisted by a multi-sector BD-RIS operating in time-switching (TS) mode. Specifically, we derive closed-form expressions for the moment-generating function (MGF), probability density function (PDF), and cumulative density function (CDF) of the signal-to-noise ratio (SNR) per user. Furthermore, exact closed-form expressions for the outage probability, achievable spectral and energy efficiency, symbol error probability, and diversity order for the proposed system model are derived. To evaluate the performance of multi-sector BD-RISs, we compare them with the simultaneously transmitting and reflecting (STAR)-RISs, which can be viewed as a special case of multi-sector BD-RIS with only two sectors. Interestingly, our analysis reveals that, for a fixed number of configurable elements, increasing the number of sectors improves outage performance while reducing the diversity order compared to the STAR-RIS configuration. This trade-off is influenced by the Rician factors of the cascaded channel and the number of configurable elements per sector. However, this superiority in slope is observed at outage probability values below 10^{-5}, which remains below practical operating ranges of communication systems. Additionally, simulation results are provided to validate the accuracy of our theoretical analyses. These results indicate that increasing the number of sectors in multi-sector BD-RIS-assisted systems significantly enhances performance, particularly in both spectral and energy efficiency gains. For instance, our numerical results show an average increase of 184% in spectral efficiency and 128% in maximum energy efficiency when transitioning from a 2-sector to a 6-sector configuration.**

***Index Terms*—Beyond diagonal reconfigurable intelligent surface (BD-RIS), full-space coverage, multi-sector RIS, performance analysis, time switching mode.**

I. Introduction

concept of the smart radio environment has been a focal point in recent discussions on the evolution of 6G wireless communications and the shaping of future wireless networks. Central to this visionary landscape is the transformative potential of reconfigurable intelligent surfaces (RISs) [2]. These innovative surfaces provide a paradigm shift in configuring the propagation conditions for information-bearing signals, leading to new challenges in the design of wireless communications systems. Specifically, these surfaces, consisting of arrays of closely spaced elements, are designed to manipulate electromagnetic waves by controlling the individual phase, amplitude, and polarization of the elements [3]. By strategically adjusting these properties, RISs can effectively steer signals, mitigate interference, extend coverage, and enhance both spectral and energy efficiency within wireless networks [4], [5]. Their programmable nature promises to ameliorate wireless communication by offering high adaptability and flexibility in optimizing signal propagation and system performance [6].

Several types of RIS architectures have emerged to cater to the evolving needs of communication systems. For instance, stacked intelligent metasurfaces (SIM) represent a notable advancement, wherein multiple layers of reconfigurable elements are stacked to achieve enhanced beamforming capabilities and more intricate wavefront manipulation [7]. Further, simultaneously transmitting and reflecting (STAR) RISs introduce a new concept by supporting both reflective and transmissive modes concurrently. This innovation extends the scope of RIS functionality, enabling full-space coverage and dynamic adaptation to varying channel conditions [8]. Beyond-Diagonal RIS (BD-RIS) technology further pushes the boundaries of RIS capabilities by relaxing the constraints of traditional surfaces with diagonal phase shift matrices [9]. BD-RISs enable more flexible beam management and improved spatial diversity through interconnection among surface elements beyond the conventional RIS structure. These advancements emphasize the continuous evolution of RIS technology towards more sophisticated, versatile, and high-performance communication solutions.

From an implementation standpoint, RISs can be categorized into three architectures based on circuit topology: single-, group-, and fully-connected architectures [10]. The single-connected design, typical of traditional RISs, features non-interconnected components and has been extensively studied in existing literature. In contrast, group- or fully-connected designs, where subsets or all RIS elements are interconnected, offer enhanced potential for exploiting channel diversity. These interconnected designs hold promise for substantial improvements in system spectral and energy efficiency gains [9]. These advanced architectures, termed as BD-RISs, allow the phase shift matrix representing the reflective coefficients of the

The authors are with the Interdisciplinary Centre for Security, Reliability and Trust (SnT), University of Luxembourg, Luxembourg. Corresponding author: *Mostafa Samy (mostafa.samy@uni.lu)*.

This work was supported by the Luxembourg National Research Fund (FNR) through the AFR Project CEP-MBD-CRIS, Grant reference 17974844.

This work in part was submitted to the the IEEE 25th International Workshop on Signal Processing Advances in Wireless Communications (SPAWC), 2024 [1]

RIS to extend beyond a diagonal structure. Nevertheless, the adoption of group/fully-connected architectures in BD-RISs introduces increased circuit complexity and control overhead.

A. Beyond Diagonal RIS

In recent literature, studies have investigated the design, optimization, and deployment strategies of different types of BD-RIS architectures, reflecting the growing interest in this innovative technology. For wide-band communication systems aided by BD-RIS, [11] introduced a model to account for the response fluctuations of BD-RIS across signals of varying frequencies. Additionally, [12] optimized the BD-RIS configuration to maximize channel capacity, assuming linear variations in BD-RIS phase-shifts across subcarriers. Reference [13] proposed a two-stage beamforming approach to jointly optimize the active beamforming at the base station (BS) and passive beamforming at the BD-RIS in order to enhance the sum-rate for a multi-user BD-RIS-assisted network. In [14], the authors presented a generalized frequency-dependent reflection model for configuring fully-connected and group-connected RISs within multi-band multi-cell multiple-input multiple-output (MIMO) networks.

Furthermore, the BD-RIS scattering matrix for an integrated sensing and communication (ISAC) system was studied in [15] to maximize the weighted sum of the signal-to-noise ratio (SNR) at both the radar receiver and communication users. Reference [16] optimized the BD-RIS scattering matrix to maximize the received signal power for single-user single-input single-output (SISO) systems, single-user MIMO and multi-user multiple-input single-output (MISO) aided BD-RIS systems. The work in [17] optimized the group- and fully-connected BD-RIS scattering matrix with discrete values, where the RIS impedance matrix is independently discretized. The work in [18] investigated a scenario where a cell-free massive MIMO system aided by BD-RIS serves two groups of users; information users and energy users for simultaneous wireless information and power transfer (SWIPT) systems. In [19], the performance of various RIS technologies, including regular (reflective and passive), STAR, and multi-sector BD-RIS, was investigated in multi-user MIMO OFDM broadcast channels.

Moreover, [20] proposed the concept of distributed BD-RIS, where the elements are spread over a wide region, contrasting with localized RIS. Reference [21] developed a BD-RIS-UAV system, deploying multiple BD-RISs on unmanned aerial vehicles (UAVs) within Mobile Edge Computing (MEC) networks. [22] introduced a dual-function radar-communication (DFRC) aided BD-RIS system to enhance communication capacity and sensing precision, thereby improving coverage for both functions. For the grouping strategy of the BD-RIS elements in the group-connected architecture, a static and dynamic method based on channel statistics and the channel state information (CSI) adaptation were proposed in [23] and [24], respectively. Similarly, a grouping scheme for BD-RIS elements is developed in [25], considering user scheduling and the optimal rate-splitting power-splitting ratio for BD-RIS aided rate-splitting multiple access (RSMA) within multi-user MIMO systems.

B. Multi-sector BD-RIS

To enable additional beam control flexibility for BD-RIS, the concept of *multi-sector BD-RIS* was introduced in [26], leveraging group-connected reconfigurable impedance networks and antenna array arrangements, as illustrated in Fig. 1. The multi-sector BD-RIS offers flexible deployment options and is particularly advantageous in millimeter wave scenarios and cell-free networks. In this context, STAR-RIS can be viewed as a particular case of a group-connected architecture, specifically when the group size is set to 2. Moreover, [27] examined the integration of multi-sector BD-RISs with rate-splitting multiple access (RSMA), demonstrating that this synergy significantly enhances system performance and extends coverage. Reference [28] exploited the multi-sector BD-RIS to user always communicates with half of the sectors of the RIS regardless of the number of elements in each sector. to provide more flexibility in terms of configuring the RIS sectors to enhance the system performance. The authors in [29] investigated multi-sector BD-RIS for wireless sensing and localization, proposing a self-sensing system that uses the multi-sector BD-RIS geometry to scatter signals for full-space coverage.

C. Motivation and Contributions

From the aforementioned studies, it is evident that important progress has been made in optimizing BD-RIS communication networks. However, there is still a gap in offering a thorough performance analysis for multi-sector BD-RIS across different fading scenarios. Hence, this paper presents a comprehensive investigation into the impact of dividing a fixed number of configurable elements across multiple sectors on key performance metrics of the wireless communication system, including outage probability, symbol error probability (SEP), spectral and energy efficiency, and diversity order to explore their potential performance enhancements. To achieve this, we adopt a cell-wise single-connected multi-sector BD-RIS architecture, similar to [26], [27], to ensure analytically tractable closed-form expressions. This architecture is based on a group-connected reconfigurable impedance network with a group size equal to L [26]. This analysis of the multi-sector BD-RIS across different fading channels has not been previously studied in the open literature. Specifically, we investigate a multi-sector BD-RIS-assisted network comprising L sectors, each of which containing M configurable elements. Our study provides exact closed-form expressions for the optimal SNR statistics, including probability density function (PDF), cumulative distribution function (CDF), and moment generating function (MGF). The key contributions of this paper can be outlined as follows.

1) Investigate a multi-sector BD-RIS-aided communication system operating with the time switching (TS) protocol. Within this framework, we explore diverse performance metrics while keeping the number of configurable elements at the BD-RIS constant. We analyze the impact of increasing the number of sectors, consequently reducing the number of elements per sector, in comparison to configurations with fewer sectors but more elements per

sector. We also include the STAR-RIS architecture as a reference point, treating it as a special instance of the multi-sector BD-RIS when $L = 2$.

2) Leveraging the gamma matching method, we provide expressions for various important statistics of the received SNR per user, including the CDF, PDF, and MGF over the Rician fading channels. Then, we derive closed-form expressions of the spectral efficiency and outage probability. Additionally, we compute the asymptotic outage probability for high-SNR and determine the associated diversity orders.
3) Using an MGF-based approach, we present a closed-form expression for SEP of the studied system for binary phase shift keying (BPSK) modulation scheme serving as a representative example. We also perform a high-SNR asymptotic analysis to gain further insights into SEP performance.
4) We develop a power consumption model for the multi-sector BD-RIS operating in TS mode, which incorporates the hardware power consumption at all system components, including the transmitter, receiver, and BD-RIS elements. Through this model, we evaluate the energy efficiency of the communication system.
5) Provide comprehensive numerical simulations to substantiate our analytical findings and obtain practical insights into system design considerations.

D. Paper organization

The rest of the paper is organized as follows: The considered system model is described in Section II. In Section III performance analysis is carried out to obtain closed form-expressions for the PDF, CDF, MGF, outage probability, SEP, spectral and energy efficiency, and diversity order. In Section IV, numerical results are provided. Finally, conclusions are drawn in Section V.

E. Notation

A^T denotes the transpose of A. The notation $A \sim \mathcal{CN}(\mu_A, \sigma_A^2)$ denotes that A is a circularly symmetric complex Gaussian distributed with μ_A mean and σ_A^2 variance. Further, $\text{diag}(\boldsymbol{A})$ describes a vector with elements equal to the diagonal elements of $\boldsymbol{A}$. The notation $\Pr[.]$ is the probability operation. The PDF of a random variable (RV) X is denoted by $f_X(\cdot)$, and its CDF is denoted by $F_X(\cdot)$, respectively. $\mathbb{E}[.]$ and $\mathbb{V}\text{ar}[.]$ are the expectation and variance operators, respectively.

II. System Model

As shown in Fig. 1, we consider a multi-sector BD-RIS-assisted communication system that consists of a BS and a multi-sector BD-RIS with L sectors to serve K users distributed randomly across the coverage areas of these sectors. We denote $\mathcal{K} = \{1, \ldots, K\}$, and $\mathcal{L} = \{1, \ldots, L\}$ as the set of indices of users, and sectors, respectively. This system operates under the assumption that direct links between the BS and users are obstructed due to severe blockage or the unfavorable propagation environment. Moreover, it is assumed that the BS as well as U_{k_l} are equipped with a single antenna[1]. We adopt the TS protocol for the multi-sector BD-RIS configuration, where each user U_{k_l} is accommodated in a dedicated orthogonal time slot, with its corresponding sector activated. To comprehend the concepts and terminology pertaining to multi-sector BD-RIS, we provide next a concise overview of its fundamental operational principles.

A. Multi-Sector BD-RIS: Model and Setup

The multi-sector BD-RIS is modeled as a polygon that consists of L identical sectors and an M-cell RIS [26]. We denote $\mathcal{M} = \{1, \ldots, M\}$, and $\mathcal{K}_l = \{1, \ldots, K_l\}$ as the set of indices of cells, and users located in the coverage region of sector $l, \forall l \in \mathcal{L}$ with $0 < K_l < K$, and $\sum_l K_l = K$, respectively. Based on the main characteristics of multi-sector BD-RIS, the M-cell RIS is modeled as LM elements connected to an ML-port reconfigurable impedance network, and uniformly divided into the L sectors. Each cell consists of L elements deployed at the side of the polygon while covering the whole azimuth space. In particular, cell m includes elements in the set $\mathcal{L}_m = \{m, M+m, \ldots, (L-1)M+m\}$ [26]. The elements are interconnected by reconfigurable impedance components, and thus, enable the support of the multi-sector mode. Specifically, sector l covers $1/L$ space containing elements which belongs to $\mathcal{M}_l = \{(l-1)M + 1, ..., lM\}$, $\forall l \in \mathcal{L} = \{1, \ldots, L\}$. The BS is located within the coverage of sector 1 of the multi-sector BD-RIS. Moreover, the BS is out of the coverage of the uni-directional radiation pattern of sector l of the multi-sector BD-RIS, $\forall l \in \mathcal{L}, l \neq 1$, [26]. Therefore, the multi-sector BD-RIS involves L matrices denoted as $\boldsymbol{\Phi}_l \in \mathbb{C}^{M \times M}$ for each sector l. Based on the cell-wise single-connected architecture, $\boldsymbol{\Phi}_l$, $\forall l \in \mathcal{L}$ can be modeled as diagonal matrices as follows [26]

$$\boldsymbol{\Phi}_l = \text{diag}(\phi_{(l-1)M+1}, \ldots, \phi_{lM}), \quad \forall l \in \mathcal{L}, \tag{1}$$

In the case of cell-wise single-connected architecture, constraint (1) can be expressed as [26]

$$\sum_{i \in \mathcal{L}_m} |\phi_i|^2 = 1, \ \forall m \in \mathcal{M}. \tag{2}$$

Assuming phase shifters with infinite resolution, where both the amplitude and phase shift can take continuous values, (2) can be reformulated as:

$$\begin{aligned} &\phi_i = \sqrt{\beta_i} e^{j\vartheta_i}, \forall i \in \mathcal{L}_m, \forall m \in \mathcal{M}, \\ &0 \leq \beta_i \leq 1, \forall i \in \mathcal{L}_m, \forall m \in \mathcal{M}, \\ &\sum_{i \in \mathcal{L}_m} \beta_i = 1, \forall m \in \mathcal{M}, \\ &0 \leq \vartheta_i < 2\pi, \forall i \in \mathcal{L}_m, \forall m \in \mathcal{M}. \end{aligned} \tag{3}$$

B. Channel Model

The channel vectors between the BS and the sector of the BD-RIS facing the BS, and the BD-RIS and U_{k_l} are

[1]This study focuses on analyzing the performance of multi-sector BD-RIS-assisted communications. Future work will extend this analysis to scenarios involving multiple antennas to further enhance system performance.

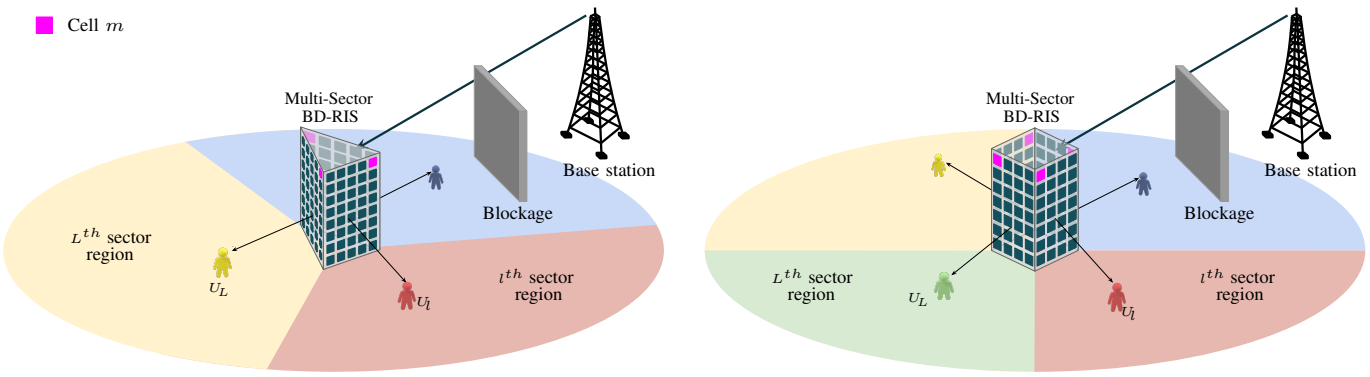

(a) $L = 3$ Multi-sector BD-RIS

(b) $L = 4$ Multi-sector BD-RIS

Fig. 1. Multi-sector BD-RIS-aided communication system

denoted by $\mathbf{h} \in \mathbb{C}^{M\times 1}$ and $\mathbf{g}_{k_l} \in \mathbb{C}^{1\times M}$, respectively, where $\mathbf{h} = [h_1, ..., h_m, ..., h_M]^{\mathrm{T}}$, while the channel vector between the l^{th} sector of the BD-RIS and U_{k_l} is denoted as $\mathbf{g}_{k_l} \in \mathbb{C}^{1\times M}$, where and $\mathbf{g}_{k_l} = [g_{k_l,1}, ..., g_{k_l,m}, ..., g_{k_l,M}]$. In this, h_m, and $g_{k_l,m}$ capture the corresponding small-scale fading coefficients. Further, Rician fading is assumed for all channels, and thus, the small-scale coefficients to and from the BD-RIS m^{th} cell are $h_m = \zeta_m e^{-j\varrho_m}$ and $g_{k_l,m} = \xi_{k_l,m} e^{-j\upsilon_{k_l,m}}$, respectively, where ζ_m and $\xi_{k_l,m}$ are the amplitude coefficients, while ϱ_m and $\upsilon_{k_l,m}$ are the phase shifts. Further, we denote α_{k_l} as the cascaded channel large-scale fading coefficient expressed as [26]:

$$\alpha_{k_l} = \frac{\lambda^4 G_t G_r}{4^3\pi^4 d_{\mathrm{RIS}}^{\eta_{\mathrm{RIS}}} d_{k_l}^{\eta_{k_l}} \left(1 - cos\frac{\pi}{L}\right)^2}, \tag{4}$$

where d_{RIS} and d_{k_l} are the distances between the BS and the BD-RIS, and the BD-RIS and U_{k_l}, respectively, while η_{RIS} and η_{k_l} are the corresponding path-loss exponents. In (4) λ represents the wavelength of transmit signal, G_t denotes the transmit antenna gain, and G_r denotes the receive antenna gain. Moreover, since we are focusing on studying the theoretical limits of this system model, and considering the channel estimation methods that have been recently developed in [23] and [24], it is assumed that the BS can acquire accurate CSI.

C. Signal Model

The received signal at user U_{k_l} randomly located within the l^{th} sector coverage region of the BD-RIS is given by

$$y_{k_l} = \mathbf{g}_{k_l} \mathbf{\Phi}_l \mathbf{h} \sqrt{p_{k_l}\, \alpha_{k_l}} s_{k_l} + n_{k_l}, \tag{5}$$

where s_{k_l} is the message of U_{k_l}, satisfying $\mathbb{E}\left[|s_{k_l}|^2\right] = 1$ [30], p_{k_l} is the transmit power, and $n_{k_l} \sim \mathcal{CN}(0, \sigma^2_{n_{k_l}})$ is the additive white Gaussian noise (AWGN) at U_{k_l}. Therefore, the received SNR of U_{k_l} is given by

$$\gamma_{k_l} = \rho_{k_l} |\mathbf{g}_{k_l} \mathbf{\Phi}_l \mathbf{h}|^2 \alpha_{k_l}, \tag{6}$$

where $\rho_{k_l} = \frac{p_{k_l}}{\sigma^2_{n_{k_l}}}$ is the transmit SNR per user. Accordingly, the system overall spectral efficiency can be given as

$$\mathcal{R} = \frac{1}{K} \sum_{l=1}^{L} \sum_{k=1}^{K_l} \log_2 (1 + \gamma_{k_l}), \tag{7}$$

where the pre-log factor $\frac{1}{K}$ is included to account for the division of the total available time among the K users, as dictated by the TS protocol.

III. Performance Analysis

In this section, our investigation begins with identifying the optimal phase shift configuration for the multi-sector BD-RIS to maximize its cascaded channel gains. Subsequently, we conduct statistical analyses for the optimal received SNR, deriving closed-form expressions for the PDF, CDF, and MGF of the multi-sector BD-RIS-aided system. Moreover, we study various system performance metrics, including outage probability, spectral and energy efficiency, diversity order, SEP, and its asymptotic analysis. To comprehensively explore these aspects, we derive closed-form expressions, providing a thorough examination of the system behavior.

A. Optimal BD-RIS Configuration

Since TS is utilized, where each user is served exactly once in a time, the maximum received signal power for U_{k_l} within the coverage of sector l', $\forall l' \in L$ at the time period $1/K$, can be achieved by activating its corresponding sector [26]. In this case, we have

$$\mathbf{\Phi}_l = \begin{cases} \mathrm{diag}(\phi_{(l-1)M+1}, \ldots, \phi_{lM}), & l = l', \\ 0, & l \neq l', \end{cases} \tag{8}$$

with $|\phi_j| = 1$, $\forall j \in M_{l'}$. Hence. the optimal phase-shifts design for $\boldsymbol{\phi}_{l'}$ can be given as follows [26]

$$\phi_{(l'-1)M+m} = -\angle[\mathbf{h}^{\mathrm{T}}]_m [\mathbf{g}_{k_{l'}}]_m \tag{9}$$

Upon implementing the optimal phase shifts $\phi_{(l'-1)M+m}$ from (9), the cascaded channel for $U_{k_{l'}}$ can be expressed as:

$$\begin{aligned}\left|\mathbf{h}_l^{\mathrm{T}}\mathbf{\Phi}_l\,\mathbf{g}_{k_{l'}}\right|^2 &= \left|\sum_{m=1}^{M} h_m g_{k_{l'},m}\right|^2 \\ &= \left(\sum_{m=1}^{M} |\zeta_m||\xi_{k_{l'},m}|\right)^2 \\ &= \left(\sum_{m=1}^{M} Y_{k_{l'},m}\right)^2 = Y_{k_{l'}}^2. \end{aligned} \tag{10}$$

B. Statistics of the Optimal Received SNR

We utilize the moment matching method to derive closed-form expressions characterizing the distribution of γ_{k_l}. This method is widely employed to approximate complex distributions [31], [32], [33], [34] by matching the moments of the target distribution with those of a simpler distribution[2]. Based on this method, the following Lemma gives the CDF, PDF and MGF of γ_{k_l}.

Lemma 1. *For a multi-sector BD-RIS operating over Rician fading channels, the CDF, PDF and MGF of γ_{k_l} can be, respectively, given as follows*:

$$F_{\gamma_{k_l}}(y) = \frac{1}{\Gamma(k_{Y_{k_l}^2})}\gamma\left(k_{Y_{k_l}^2}, \frac{y}{\alpha_{k_l}\rho_{k_l}\theta_{Y_{k_l}^2}}\right), \tag{11}$$

$$f_{\gamma_{k_l}}(y) = \frac{y^{k_{Y_{k_l}^2}-1}e^{-\frac{y}{\alpha_{k_l}\rho_{k_l}\theta_{Y_{k_l}^2}}}}{\Gamma(k_{Y_{k_l}^2})\left(\alpha_{k_l}\rho_{k_l}\theta_{Y_{k_l}^2}\right)^{k_{Y_{k_l}^2}}}, \tag{12}$$

and

$$M_{\gamma_{k_l}}(s) = \left(1 - s\rho_{k_l}\alpha_{k_l}\theta_{Y_{k_l}^2}\right)^{-k_{Y_{k_l}^2}}, \tag{13}$$

where $\Gamma(.)$ is the Gamma function, $\gamma(\cdot,\cdot)$ is the lower incomplete gamma function [37],

$$k_{Y_{k_l}^2} = \frac{\mathbb{E}[Y_{k_l}^2]^2}{\mathbb{V}\mathrm{ar}[Y_{k_l}^2]}, \tag{14}$$

$$\theta_{Y_{k_l}^2} = \frac{\mathbb{V}\mathrm{ar}[Y_{k_l}^2]}{\mathbb{E}[Y_{k_l}^2]}, \tag{15}$$

$$\mathbb{E}[Y_{k_l}^2] = \frac{\Gamma(k_{Y_{k_l}}+2)}{\Gamma(k_{Y_{k_l}})}\theta_{Y_{k_l}}^2, \tag{16}$$

$$\mathbb{V}\mathrm{ar}[Y_{k_l}^2] = \left(\frac{\Gamma(k_{Y_{k_l}}+4)}{\Gamma(k_{Y_{k_l}})} - \frac{\Gamma(k_{Y_{k_l}}+2)^2}{\Gamma(k_{Y_{k_l}})^2}\right)\theta_{Y_{k_l}}^4, \tag{17}$$

$$k_{Y_{k_l}} = \frac{\mathbb{E}[Y_{k_l}]^2}{\mathbb{V}\mathrm{ar}[Y_{k_l}]}, \tag{18}$$

$$\theta_{Y_{k_l}} = \frac{\mathbb{V}\mathrm{ar}[Y_{k_l}]}{\mathbb{E}[Y_{k_l}]}, \tag{19}$$

$$\mathbb{E}[Y_{k_l}] = \frac{M\pi L_{\frac{1}{2}}(-\kappa_h)L_{\frac{1}{2}}(-\kappa_g)}{4\sqrt{(\kappa_h+1)(\kappa_g+1)}}, \tag{20}$$

$$\mathbb{V}\mathrm{ar}[Y_{k_l}] = M - \frac{M\pi^2 L_{\frac{1}{2}}(-\kappa_h)^2 L_{\frac{1}{2}}(-\kappa_g)^2}{16(\kappa_h+1)(\kappa_g+1)}. \tag{21}$$

Proof: Please refer to Appendix A. ■

Lemma 1. is verified in Fig. 2, where the CDF and MGF of γ_{k_l} are validated through Monte Carlo simulation, while the PDF through the kernel density estimation (KDE) method. As shown, the simulation and the analytical results match perfectly.

C. Spectral Efficiency

The achievable spectral efficiency can be obtained as

$$\mathcal{R} = \mathbb{E}\left[\frac{1}{K}\sum_{l=1}^{L}\sum_{k=1}^{K_l}\log_2\left(1+\gamma_{k_l}\right)\right]. \tag{22}$$

By using Jensen's inequality, a lower bound of the spectral efficiency in (22) is given by

$$\mathcal{R} \geq \tilde{\mathcal{R}} = \frac{1}{K}\sum_{l=1}^{L}\sum_{k=1}^{K_l}\log_2\left(1+\mathbb{E}[\gamma_{k_l}]\right). \tag{23}$$

which can be obtained in closed-form as

$$\mathcal{R} = \frac{1}{K}\sum_{l=1}^{L}\sum_{k=1}^{K_l}\log_2\left(1+\frac{\rho_{k_l}\alpha_{k_l}\Gamma(k_{Y_{k_l}}+2)}{\Gamma(k_{Y_{k_l}})}\theta_{Y_{k_l}}^2\right). \tag{24}$$

Proposition 1. *For a fixed number of configurable elements, the impact of beam directivity outweighs that of BD-RIS sector dimensions. For instance, a 6-sectors BD-RIS provides higher spectral efficiency than that of a 2-sectors setup, where the expressions of spectral efficiency for 2- and 6-sectors BD-RIS are respectively given as:*

$$\mathcal{R} = \frac{1}{K}\sum_{l=1}^{L}\sum_{k=1}^{K_l}\log_2\left(1+A\left[0.25Z^2\Omega + 0.5Z(1-\Omega)\right]\right), \tag{25}$$

$$\mathcal{R} = \frac{1}{K}\sum_{l=1}^{L}\sum_{k=1}^{K_l}\log_2\left(1+A\left[1.54Z^2\Omega + 9.28Z(1-\Omega)\right]\right), \tag{26}$$

where Z is the total number of configurable elements for the whole BD-RIS, i.e., $Z = LM$,

$$\Omega = \frac{\pi^2 L_{\frac{1}{2}}(-\kappa_h)^2 L_{\frac{1}{2}}(-\kappa_g)^2}{16(\kappa_h+1)(\kappa_g+1)}, \text{and} \tag{27}$$

$$A = \frac{\rho_{k_l}\lambda^4 G_t G_r}{4^3\pi^4 d_a^{\eta_a} d_b^{\eta_b}}. \tag{28}$$

Proof: Please refer to Appendix B. ■

[2]Previous works that utilized the gamma moment matching as in [31], [32], [33], [34] or the Laguerre series method as in [35] and [36], typically involved a random variable transformation, which often resulted in the random variables that are no longer adhering to a gamma distribution. Herein, as detailed in Appendix A, our approach retains γ_{k_l} as a gamma distribution, enabling the derivation of a novel closed-form expression for the MGF. Consequently, our approach provide simple yet accurate statistical characterizations, and favorable for further analysis as will be demonstrated in the next subsections.

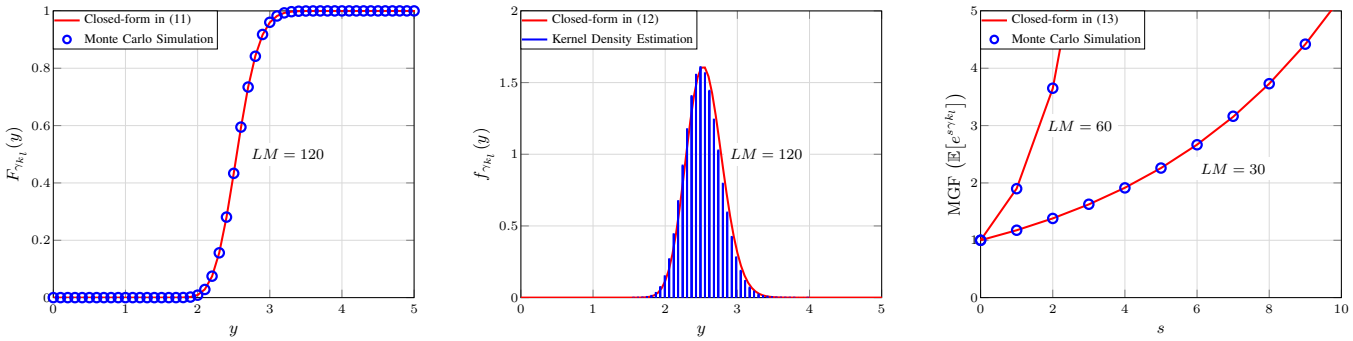

(a) CDF validation of γ_{k_l} in (11)

(b) PDF validation of γ_{k_l} in (12).

(c) MGF validation of γ_{k_l} in (13)

Fig. 2. Verification of Lemma 1. for $L = 3$, $p_{k_l} = 30$, $\kappa_h = \kappa_g = 10$, and the rest of the parameters are provided in Table I in the Numerical section.

Remark 1. *While increasing the number of sectors enhances spectral efficiency for a given number of configurable elements, it comes at the cost of higher hardware complexity due to the increased interconnections of the configurable impedance within each cell, highlighting a crucial tradeoff between performance and hardware complexity.*

D. Outage Probability

Outage probability represents the likelihood that a user link fails to meet a certain predefined quality-of-service (QoS) requirement [38]. In this system model, the QoS requirement is specified in terms of a minimum SNR that is given in (6). Thus, a user's outage probability can be expressed as

$$\begin{aligned} \mathrm{P}_{k_l}(\mathcal{O}) &= \Pr\left[\gamma_{k_l} \leq \psi_{k_l}\right] \\ &= F_{\gamma_{k_l}}(\psi_{k_l}), \end{aligned} \tag{29}$$

where $\psi_{k_l} = 2^{KR_{k_l}} - 1$. Substituting the CDF in (11) into (29), the outage probability closed-form expression can be given as

$$\mathrm{P}_{k_l}(\mathcal{O}) = \frac{1}{\Gamma(k_{Y^2_{k_l}})} \gamma\left(k_{Y^2_{k_l}}, \frac{\psi_{k_l}}{\alpha_{k_l}\rho_{k_l}\theta_{Y^2_{k_l}}}\right). \tag{30}$$

Corollary 1. *The outage performance of a 6-sector BD-RIS is expected to surpass that of a 2-sector BD-RIS. This inference stems from the observation that increasing the number of sectors results in improved achievable spectral efficiency.*

E. Diversity Order

The diversity order represents the rate at which the outage probability decreases as the SNR increases. It quantifies the system resilience to fading, indicating how effectively the system can exploit diversity techniques to combat channel impairments. A higher diversity order implies faster outage probability decay, indicating better performance in challenging communication environments. Specifically, the diversity order represents the negative slope of the outage probability as the SNR approaches infinity [39]. Moreover, the outage probability can be asymptotically represented as $\mathrm{P}_{k_l} \approx (G_c\rho_{k_l})^{-G_d}$, where G_d is the diversity order and G_c is a measure of the coding gain [39]. The analytical expression for $\mathrm{P}_{k_l}(\mathcal{O})$ can be given by

$$\mathrm{P}^{\infty}_{k_l}(\mathcal{O}) = \left[\frac{\alpha_{k_l}\theta_{Y^2_{k_l}}\rho_{k_l}}{\psi_{k_l}\Gamma\left(k_{Y^2_{k_l}}+1\right)^{\frac{-1}{k_{Y^2_{k_l}}}}}\right]^{-k_{Y^2_{k_l}}}, \tag{31}$$

where the coding gain is $G_c = \left[\frac{\alpha_{k_l}\theta_{Y^2_{k_l}}}{\psi_{k_l}\Gamma\left(k_{Y^2_{k_l}}+1\right)^{\frac{-1}{k_{Y^2_{k_l}}}}}\right]$, and the diversity order is $G_d = k_{Y^2_{k_l}}$.

Proof: The lower incomplete gamma function can be expanded as follows [37, Eq. (8.354.1)]

$$\gamma(k_{Y^2_{k_l}}, \frac{\psi_{k_l}}{\rho_{k_l}\alpha_{k_l}\theta_{Y^2_{k_l}}}) = \sum_{n=0}^{\infty} \frac{(-1)^n \left(\frac{\psi_{k_l}}{\rho_{k_l}\alpha_{k_l}\theta_{Y^2_{k_l}}}\right)^{k_{Y^2_{k_l}}+n}}{n!(k_{Y^2_{k_l}}+n)}. \tag{32}$$

At high SNR, ρ_{k_l} approaches ∞. Therefore, the first term in the summation in (32) is the dominate one, and by considering this, we have:

$$\gamma(k_{Y^2_{k_l}}, \frac{\psi_{k_l}}{\rho_{k_l}\alpha_{k_l}\theta_{Y^2_{k_l}}}) = \frac{\left(\frac{\psi_{k_l}}{\rho_{k_l}\alpha_{k_l}\theta_{Y^2_{k_l}}}\right)^{k_{Y^2_{k_l}}}}{k_{Y^2_{k_l}}}, \tag{33}$$

substituting (33) into (30) and applying some algebraic manipulation we obtain (31). ■

Remark 2. *The diversity order $k_{Y^2_{k_l}}$ is dependent on various factors including the number of configurable elements per sector M, and the Rician channel factors κ_h and κ_g, i.e. the LoS connection establishment through the deployment of the BD-RIS. These parameters collectively influence the system ability to achieve diversity gain, highlighting the significance of their careful consideration in the design and deployment of the BD-RIS-aided networks.*

Remark 3. *Although designing a multi-sector BD-RIS with a high number of sectors achieves better outage performance than with a low number of sectors for a given number of configurable elements, it becomes evident that a higher diversity order is obtained with a low number of sectors compared to a high number. This is because the diversity order is dependent on the number of configurable elements per sector.*

F. Symbol Error Probability

In this subsection, we analyze the SEP, a critical metric for evaluating the system performance. SEP quantifies the likelihood of erroneous detection or reception of symbols in digital communication systems. It represents the probability that a transmitted symbol is incorrectly decoded or received as a different symbol due to noise or other impairments in the channel. In our system model, we leverage the MGF-based approach to compute the average SEP specifically tailored for M-phase shift keying (PSK) signaling, which is obtained as [40, Eq. (5.67)]:

$$P_s = \frac{1}{\pi}\int_0^{(M-1)\pi/M} M_{\gamma_{k_l}}\left(-\frac{2\sin^2(\pi/M)}{2\sin^2\delta}\right)d\delta, \tag{34}$$

Proposition 2. *By evaluating for BPSK ($M = 2$) as a representative example of $M-$ary modulation scheme, and substituting the MGF of (13) into (34) we have*

$$P_s = \frac{1}{\pi}\int_0^{\pi/2}\left(1+\frac{\rho_{k_l}\alpha_{k_l}\theta_{Y^2_{k_l}}}{\sin^2\delta}\right)^{-k_{Y^2_{k_l}}}d\delta, \tag{35}$$

with the help of [40, Eq. (5.17b)], we can solve the above integral, and thus, the closed-form expression for the average SEP of BPSK can be given as

$$P_s = \frac{1}{2\sqrt{\pi}}\frac{\sqrt{\rho_{k_l}\alpha_{k_l}\theta_{Y^2_{k_l}}}}{\left(1+\rho_{k_l}\alpha_{k_l}\theta_{Y^2_{k_l}}\right)^{k_{Y^2_{k_l}}+\frac{1}{2}}}\frac{\Gamma\left(k_{Y^2_{k_l}}+\frac{1}{2}\right)}{\Gamma\left(k_{Y^2_{k_l}}+1\right)} \times {}_2F_1\left(1, k_{Y^2_{k_l}}+\frac{1}{2}; k_{Y^2_{k_l}}+1, \frac{1}{1+\rho_{k_l}\alpha_{k_l}\theta_{Y^2_{k_l}}}\right), \tag{36}$$

where ${}_2F_1(.,.;.,.)$ is the Gauss hypergeometric function.

Next, we analyze the asymptotic SEP in high-SNR regimes, facilitating an insightful investigation on the system performance under favorable conditions. Leveraging the property ${}_2F_1(.,.;.,0) = 1$ [41] at high SNR, along with some algebraic manipulations, we can obtain the asymptotic SEP closed-form expression as follows:

$$P_s = \left(\alpha_{k_l}\theta_{Y^2_{k_l}}\left(\frac{2\sqrt{\pi}\Gamma\left(k_{Y^2_{k_l}}+1\right)}{\Gamma\left(k_{Y^2_{k_l}}+\frac{1}{2}\right)}\right)^{\frac{1}{k_{Y^2_{k_l}}}}\rho_{k_l}\right)^{-k_{Y^2_{k_l}}} \tag{37}$$

where the coding gain is $G_c = \left[\alpha_{k_l}\theta_{Y^2_{k_l}}\left(\frac{2\sqrt{\pi}\Gamma\left(k_{Y^2_{k_l}}+1\right)}{\Gamma\left(k_{Y^2_{k_l}}+\frac{1}{2}\right)}\right)^{\frac{1}{k_{Y^2_{k_l}}}}\right]$, and the diversity order is $G_d = k_{Y^2_{k_l}}$.

Remark 4. *The asymptotic SEP exhibits similar behavior to the asymptotic outage probability, given their shared diversity order of $k_{Y^2_{k_l}}$, which emphasizes the interrelation between these key performance metrics in evaluating system reliability and robustness.*

G. Energy Efficiency

Energy efficiency is an important metric for evaluating system performance. In this subsection, we introduce the definition and derivation of the energy efficiency for the studied system model, which is measured in bits-per-joule (b/J) and defined as

$$EE = W\frac{\mathcal{R}}{\mathcal{P}_{\text{total}}}, \tag{38}$$

where W denotes the transmission bandwidth in Hz, $\mathcal{R}$ is the spectral efficiency as defined in (24), and $\mathcal{P}_{\text{total}}$ is the total power consumed by the BD-RIS-aided communication system.

To compute the total power consumption $\mathcal{P}_{\text{total}}$ in this system, we provide a description of the energy consumption model. The network energy consumption includes the BS transmit power, alongside the hardware static power consumed by the BS, user terminals, and the BD-RIS. Hence, the total power consumption between the BS and U_{k_l} can be expressed as [42]:

$$\mathcal{P}_{k_l} = p_{k_l}/\nu + P_{\text{UE},k_l} + P_{\text{BS}} + P_{\text{RIS}}, \tag{39}$$

where P_{UE,k_l}, and P_{BS} denote the hardware static power dissipated by U_{k_l} user equipment, and total hardware static power consumption at the BS, respectively. In (39), $\nu \in (0, 1]$ accounts for the power amplifier efficiency [43]. Additionally, we make the assumption that the transmit amplifier operates within its linear range, and its circuit power remains independent of the communication rate [42]. These assumptions align with standard wireless communication systems, where amplifiers are engineered to operate within their linear transfer function region, and where the hardware-dissipated power can be represented by a constant offset [42]. With the adoption of the TS protocol, the power consumption of the BD-RIS can be attributed to three primary components. First, since only the sector corresponding to each U_{k_l} is activated at a time, there is $P_{sw\text{-}cir}$, which accounts for the power dissipation caused by the circuitry involved in switching between sectors. Secondly, an $L \times L$ switches can be implemented per cell M as shown in Fig. 3 to isolate the phase shifters of inactive sectors to provide maximum energy efficiency performance. As a result, the power dissipation due to the use of the switches during each user's orthogonal time slot can be represented by L^2MP_{sw}, where P_{sw} is the power consumed per switch. Thirdly, there is P_e which comes from the phase shift applied to each element in the activated sector as specified in (9). Hence, during each user's orthogonal time slot, the power dissipation due to phase

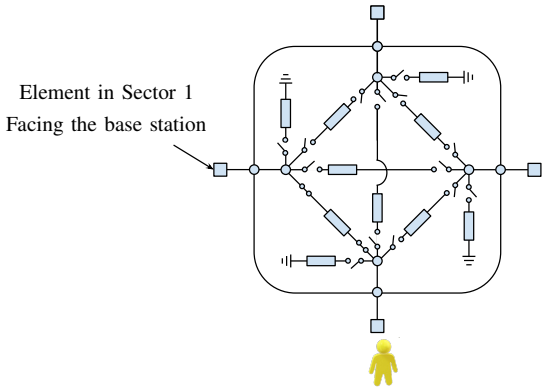

Fig. 3. An example of Cell M operation in time switching for $L = 4$ sectors; when the sector corresponding to the user is activated, switch arrays can be used to deactivate the phase shifters in other sectors to reduce the overall energy consumption.

shifting is MP_e. Consequently, the total power dissipation at the BD-RIS for all K user transmissions amounts to[3]

$$P_{\text{RIS}} = P_{sw\text{-}cir} + KMP_e + KL^2MP_{sw} \tag{40}$$

Therefore, based on the derived spectral efficiency in (24), the overall energy efficiency can be expressed as follows:

$$EE = W\frac{\frac{1}{K}\sum\limits_{l=1}^{L}\sum\limits_{k=1}^{K_l}\log_2\left(1+\frac{\rho_{k_l}\alpha_{k_l}\Gamma(k_{Y_{k_l}}+2)}{\Gamma(k_{Y_{k_l}})}\theta_{Y_{k_l}}^2\right)}{\sum\limits_{l=1}^{L}\sum\limits_{k=1}^{K_l}(p_{k_l}/\nu + P_{\text{UE},k_l}) + P_{\text{BS}} + P_{\text{RIS}}}. \tag{41}$$

IV. Numerical Results

In this section, we conduct simulations to validate the performance of the proposed system. Specifically, we numerically evaluate the derived outage probability, average spectral and energy efficiency, diversity order and SEP analytical expressions. To ensure precision, Monte Carlo simulations are performed with a total of 10^6 random Rician fading channel realizations. The targeted data rates per user R_{k_l} are measured in bits per channel use (BPCU). Unless explicitly specified, the simulation parameters are detailed in Table I.

Table I: Simulation Parameters

Parameter	Value
Transmit signal frequency f	2.4 GHz
W	10 MHz
ν	0.5
$P_{\text{UE},k} = P_{\text{BS}} = P_{sw}$	10 dBm
Bandwidth BW:	10 MHz
P_e	0.5 mW
K	6
d_{RIS}	100 m
d_{k_l}	30 m
η for Rician	2
η for Rayleigh	3
$G_t = G_r$	1
Noise power $\sigma^2_{n_{k_l}}$	-80 dBm

A. Spectral Efficiency

In Fig. 4, we investigate the spectral efficiency of the multi-sector BD-RIS assisted communication for finite number of configurable elements, set at $LM = 360$, distributed across various sector counts. As observed, a BD-RIS with $L = 6$ sectors shows a significant gain compared to a BD-RIS with $L = 2$ sectors. For example, in the case of Rician fading, achieving a spectral efficiency of 2 bit/sec/Hz demands a transmit power of $p = 16$ dBm for the 6-sector BD-RIS, whereas the same spectral efficiency requires $p_{k_l} = 24$ dBm for the 2-sector configuration, serving the same total number of users. This disparity can be attributed to the narrowing beamwidth of each BD-RIS element with increasing sector count, leading to higher directionality. Specifically, transitioning from 2 sectors to 6 sectors yields an average spectral efficiency gain of 184% for $\kappa = 10$. These findings highlight the substantial spectral efficiency gains achieved through sectorization in multi-sector BD-RIS systems, thereby maximizing channel capacity utilization, especially in Rician fading scenarios.

In Fig. 5, the spectral efficiency versus the total number of the whole BD-RIS elements is compared under different number of sectors from $L = 2$ to $L = 6$. One can observe that increasing the number of sectors has a significant effect on reducing the number of elements required to achieve a certain spectral efficiency. For instance, to realize a targeted spectral efficiency $\overline{\mathcal{R}} = 6$ bit/sec/Hz, the number of elements required for a 6-sectors BD-RIS is $LM = 330$, while the number of elements needed to achieve the same spectral efficiency increases to $LM = 800$ for a 2-sector BD-RIS.

B. Outage probability

In Fig. 6, the effect of varying the number of sectors and the Rician factors κ_h and κ_g on the outage probability for U_{k_l} is investigated. Evidently, the outage performance is significantly improved as the number of sectors or the Rician factor increases, indicating enhanced system performance attributed to the multi-sector BD-RIS implementation. This also verifies Corollary 1. Moreover, the analytical expression match perfectly with simulation curves. One can also deduce that the outage performance depends on the precise positioning of the multi-sector BD-RIS to establish virtual LoS connections between the BS and users, where this strategic placement ensures minimizing the probability of outage events.

In Fig. 7, we can observe that increasing the number of sectors notably reduces the required number of elements to attain a certain outage performance level. In particular, the multi-sector BD-RIS outperforms the STAR-RIS configuration by minimizing the number of elements needed to realize a given outage value. For instance, achieving a 10^{-2} outage probability with $L = 6$, the multi-sector setup requires approximately $M \approx 350$ elements compared to $M \approx 825$ in the STAR-RIS setup, marking a 135% reduction in required elements through sectorization of the BD-RIS. The findings emphasize the efficiency of multi-sector BD-RIS deployments in achieving outage performance targets with fewer elements compared to traditional STAR-RIS setups. This highlights the potential for significant resource savings and improved system scalability, offering a compelling advantage for practical implementation in communication networks.

C. Diversity order

In Fig. 8, we investigate the system outage performance across varying numbers of LM configurable elements and different sector counts. Clearly, the derived analytical and asymptotic expressions align closely with simulation curves, validating their accuracy in characterizing the system outage behavior. Moreover, the observed increase in diversity gain with higher numbers of elements per sector corroborates the analysis of diversity order and aligns with the insights from Remark 2 and Remark 3. Specifically, the outage probability

[3]Note that, if energy-splitting mode were employed, where all sectors are activated simultaneously, the impedance of each cell would need to be considered concurrently, potentially leading to a more complex control and power consumption model.

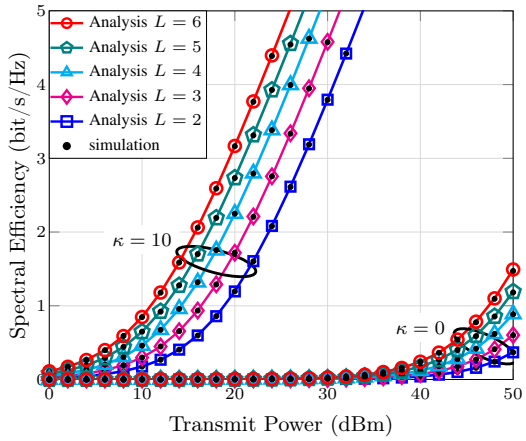

Fig. 4. Spectral efficiency versus transmit power p_{k_l} in dBm for different number of sectors with $LM = 360$ and $\kappa_h = \kappa_g = \kappa$

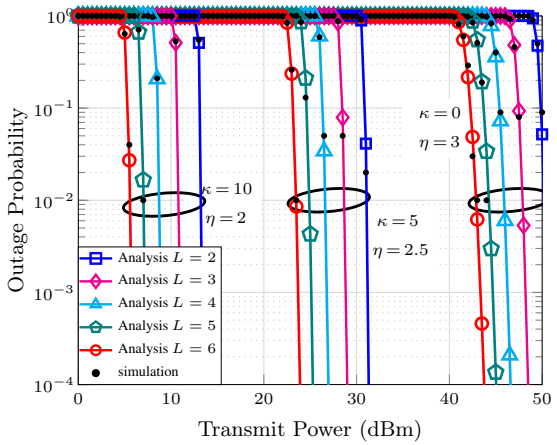

Fig. 6. Outage probability versus p_k in dBm for different number of sectors with $LM = 960$ and $\kappa_h = \kappa_g = \kappa$ for $R_{k_l} = 0.25$.

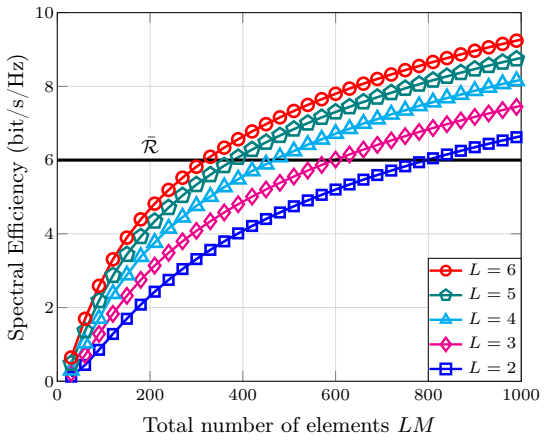

Fig. 5. Spectral efficiency vs the total number of elements for different number of sectors while fixing $LM = 360$.

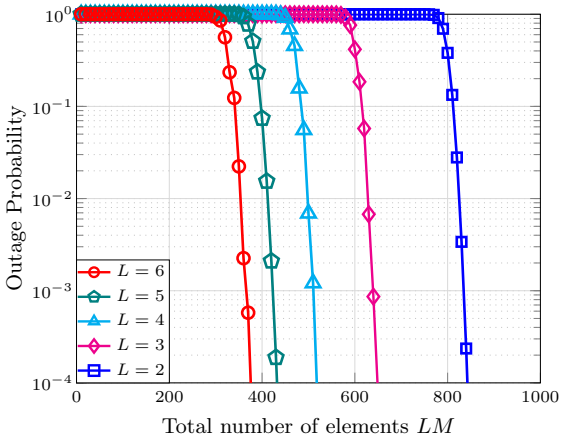

Fig. 7. Outage probability versus total number of elements LM for different number of sectors and $\kappa_h = \kappa_g = 10$ for $R_{k_l} = 0.25$.

curves exhibit a steeper slope for lower numbers of sectors, attributed to the relationship between diversity orders and the configurable elements per sector M. However, this superiority of fewer sectors is observed primarily below an outage probability of 10^{-5}, which remains below practical outage probability values typically encountered in real systems (10^{-4} to 10^{-5}). Further, increasing LM yields a notable enhancement in the outage curves, diminishing the superiority in diversity order for a low number of sectors as LM increases.

In Fig. 9, the outage and asymptotic behavior are investigated versus transmit power for different Rician factors κ_h and κ_g. Evidently, the outage performance is enhanced as the Rician factor increases, which is attributed to the presence of stronger LoS components in the communication channel, implying that the outage performance depends on the precise placement of the multi-sector BD-RIS to establish virtual LoS connections between the BS and users. This observation also validate the diversity order analysis since G_d, is a function of the Rician factors κ_h and κ_g. Furthermore, the correlation between Rician factors and the diversity order highlights their influence on system reliability, affirming the importance of accounting for channel characteristics in the design and deployment of multi-sector BD-RIS setups.

D. Symbol Error Probability

In Fig. 10, we investigate the impact of utilizing more configurable elements on the SEP performance, varying the total number of elements LM. Clearly, increasing LM and the number of sectors enhances SEP performance. Moreover, sectoriziaton of the BD-RIS yields improved SEP performance. For example, with $LM = 960$, achieving a probability value of 10^{-2} requires approximately 6.8 dBm transmit power for a 6-sector BD-RIS, whereas a 2-sector BD-RIS demands roughly 14.70 dBm, indicating a reduction in transmit power of 7.9 dBm when transitioning from 2 to 6 sectors. This considerable reduction in the required transmit power points out the efficiency gains achieved through RIS sectorization, emphasizing its potential to significantly enhance system performance while concurrently reducing power consumption.

In Fig. 11, we evaluate the SEP for the multi-sector BD-RIS under different fading conditions. Specifically, we vary the Rician factors and path loss exponents while keeping the total number of elements in the multi-sector BD-RIS fixed at $LM = 960$. Intuitively, it is clear from this result that an increase in the path loss exponent leads to degraded SEP performance. Additionally, SEP degrades with lower Rician factors. However, this degradation can be mitigated by adopting

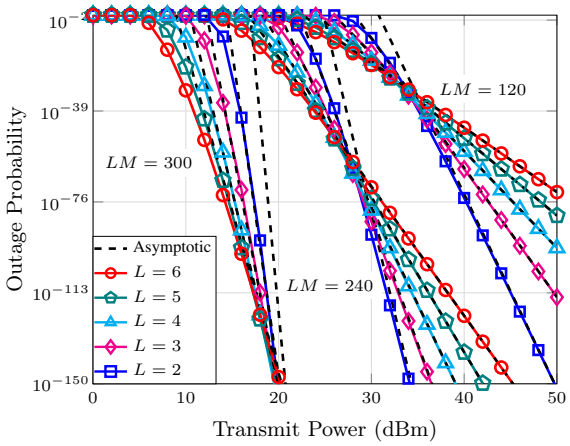

Fig. 8. Asymptotic outage analysis and simulation for muli-sector BD-RIS against transmit power for different number of sectors and different LM with $\kappa_h = \kappa_g = 10$, $d_{\text{RIS}} = 30$ m and $d_{k_l} = 30$ m, for $R_{k_l} = 0.25$.

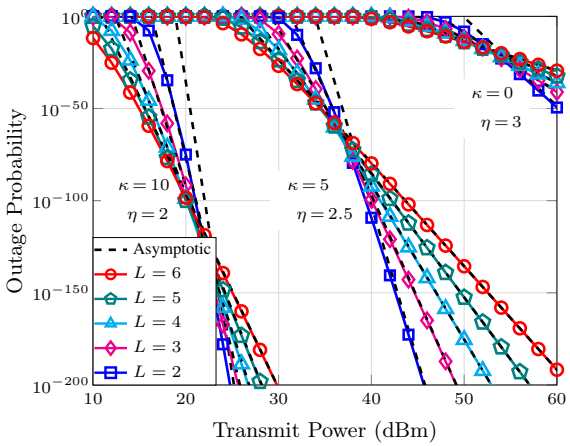

Fig. 9. Asymptotic outage analysis and simulation for muli-sector BD-RIS against transmit power for different number of sectors with $LM = 240$, $\kappa_h = \kappa_g = \kappa$, $d_{\text{RIS}} = 30$ m and $d_{k_l} = 30$ m, for $R_{k_l} = 0.25$.

solutions such as increasing transmit power and/or expanding the number of sectors in the BD-RIS. In practical systems, while increasing transmit power can provide a straightforward solution, it may lead to undesirable consequences such as increased energy consumption and interference. On the other hand, increasing the number of sectors in the BD-RIS offers a more sustainable approach, as it leverages spatial diversity to enhance communication reliability without significantly increasing energy consumption or interference levels.

Next, we evaluate the asymptotic SEP under varying channel conditions. Fig. 12 studies the impact of the total number of configurable elements LM and the Rician factors $\kappa_h = \kappa_g$ on the asymptotic SEP performance. As expected, a similar trend is observed as in the asymptotic outage probability analysis. Specifically, the diversity order G_d increases with higher Rician factors or total number of elements LM, leading to improved diversity order, consistent with the observations for outage probability. This correlation is aligned with the insights obtained in Remark 4.

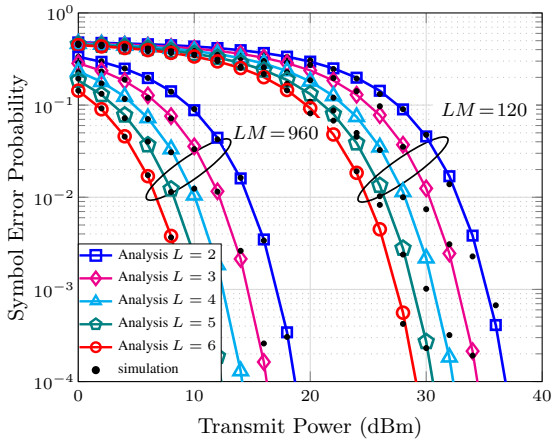

Fig. 10. SEP versus p_{k_l} in dBm for different number of configurable elements for the whole BD-RIS and $\kappa_h = \kappa_g = 10$.

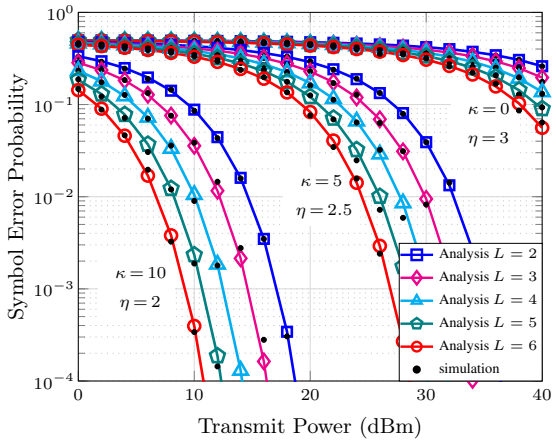

Fig. 11. SEP performance for different Rician factors $\kappa_h = \kappa_g$ and different number of sectors with fixed $LM = 960$.

E. Energy Efficiency

In Fig. 13, we investigate the energy efficiency performance of the multi sector BD-RIS. Clearly, when distributing the $LM = 360$ configurable elements across 6 sectors, significant energy efficiency enhancements are evident compared to allocating them across only 2 sectors. Specifically, when the total number of elements LM are divided into 6 sectors, the maximum energy efficiency peaks at 1.8 Mb/J with a transmit power of 28 dBm. In contrast, when limited to 2 sectors, the maximum efficiency diminishes to 0.79 Mb/J at a higher transmit power of 32 dBm. In other words, transitioning from 2 to 6 sectors yields a notable 128% increase in maximum energy efficiency, representing more than a twofold gain in system energy efficiency.

Fig. 14 depicts the achievable energy efficiency plotted against the total number of configurable elements of the entire BD-RIS LM for different number of sectors. It is evident that as LM grows, the performance of the energy efficiency curves significantly improves owing to the enhancement in spectral efficiency. However, a further increase in LM leads to a decline in the energy efficiency. This can be attributed to the fact that while the power consumption of the BD-RIS (P_{RIS}) linearly increases with LM, the spectral efficiency

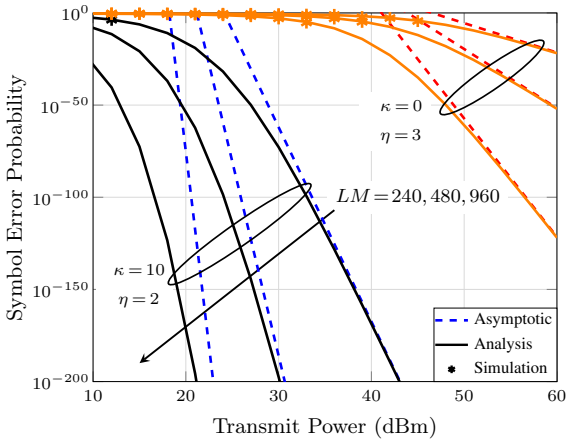

Fig. 12. Asymptotic SEP analysis and simulation for different Rician factors $\kappa_g = \kappa_h = \kappa$, and different number of configurable elements for $L = 6$.

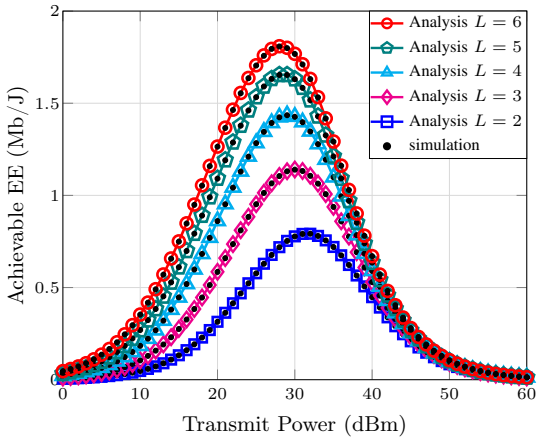

Fig. 13. Energy efficiency versus transmit power p_k for fixed total number of elements for the whole multi-sector $LM = 360$ with different number of sectors, and $\kappa_h = \kappa_g = 10$.

does not increase at the same rate. Instead, it begins to saturate, as observed in Fig. 5, particularly when there is a substantial increase in the number of configurable elements. Furthermore, it can be clearly observed that increasing the number of sectors can be a promising solution to mitigate the corresponding energy consumption associated with deploying a BD-RIS with a massive number of configurable elements. This is particularly relevant in scenarios where a large number of elements are required to counteract severe path loss, as the energy efficiency is degraded with increasing the number of elements. This result also implies the existence of a tradeoff between the number of configurable elements LM of the BD-RIS and system energy efficiency, indicating that optimization can be achieved according to the channel conditions and usage scenarios.

In closing, the obtained results in this section highlight the importance of sectorization in practical system designs leveraging multi-sector BD-RIS technology. They demonstrate the significant impact of increasing the number of sectors on spectral and energy efficiency, emphasizing the importance of carefully considering sectorization schemes for substantial performance improvements in real-world deployments. However,

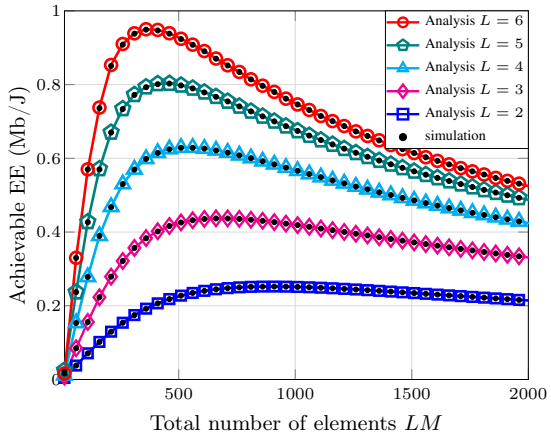

Fig. 14. Energy efficiency versus the total number of elements for the whole multi-sector LM with different number of sectors, $p_{k_l} = 17$ dBm, and $\kappa_h = \kappa_g = 10$.

it is important to mention that while increasing the number of sectors can enhance spectral and energy efficiency gains, it also introduces added hardware and control complexities. Thereby, in practical system designs, there exists a tradeoff between potential performance enhancements and the associated overhead in hardware and control intricacies.

V. Conclusions

In this paper, we conducted a comprehensive performance analysis of a multi-sector BD-RIS-assisted communication system. Specifically, we derived closed-form expressions for the MGF, PDF, and CDF of the SNR per user. Furthermore, exact closed-form expressions were derived for the outage probability, achievable spectral and energy efficiency, SEP, and diversity order for the studied system model under Rician fading channels. Our high-SNR asymptotic analysis revealed that increasing the number of sectors for a fixed number of configurable elements improves outage performance at the expense of a lower diversity order. However, this convergence occurs below outage probability of 10^{-5}. Moreover, our study provided useful insights into the nuanced performance characteristics of these systems. We found that increasing the number of sectors within the BD-RIS architecture while keeping the total number of configurable elements fixed offers a promising avenue for enhancing system performance. Numerical results demonstrated significant gains in spectral and energy efficiency when transitioning from a lower number of sectors to a higher one. These findings underscore the considerable potential of multi-sector BD-RIS configurations in optimizing spectral and energy efficiency metrics, providing valuable guidance for future system design and deployment strategies. Looking ahead, there are several promising research directions for multi-sector BD-RIS systems that can be explored for optimizing the performance and scalability of the BD-RIS architecture.

APPENDIX A

DERIVATION OF THE CDF, PDF, AND MGF OF γ_{k_l}

The mean and variance of ζ_m and $\xi_{m,k}$ can be obtained with the help of [44, Eq. (59)] by evaluating the n^{th} moment at $n=\frac{1}{2}$ and $n=1$, respectively, as follows:

$$\mathbb{E}[\zeta_m] = \sqrt{\frac{\pi}{4(\kappa_h+1)}}{}_1F_1\left(-\frac{1}{2};1;-\kappa_h\right), \tag{42}$$

$$\mathbb{V}\text{ar}[\zeta_m] = 1 - \frac{\pi}{4(\kappa_h+1)}{}_1F_1\left(-\frac{1}{2};1;-\kappa_h\right)^2, \tag{43}$$

where ${}_1F_1\left(-\frac{1}{2};1;\kappa_h\right)$ is the confluent hypergeometric function of the first kind. Note that, ${}_1F_1\left(-\frac{1}{2};1;\kappa_h\right)$ can be expressed in terms of Laguerre polynomial [45].

Similarly, $\xi_{k_l,m}$ follows a Rician distribution with the following mean and variance:

$$\mathbb{E}[\xi_{k_l,m}] = \sqrt{\frac{\pi}{4(\kappa_g+1)}}L_{\frac{1}{2}}(-\kappa_g), \tag{44}$$

$$\mathbb{V}\text{ar}[\xi_{k_l,m}] = 1 - \frac{\pi}{4(\kappa_g+1)}L_{\frac{1}{2}}(-\kappa_g)^2, \tag{45}$$

where $L_{\frac{1}{2}}(-\kappa_g) = e^{\frac{-\kappa_g}{2}}\left[(1+\kappa_g)I_0(\frac{\kappa_g}{2}) + \kappa_g I_1(\frac{\kappa_g}{2})\right]$, $I_\nu(\cdot)$ is the modified ν-order Bessel function of the first kind [37, Eq. (8.431)]. Since ζ_m and $\xi_{k_l,m}$ are independent random variables, the mean and variance of the their product can be determined as follows

$$\mathbb{E}[Y_{k_l,m}] = \mathbb{E}[\zeta_m]\mathbb{E}[\xi_{k_l,m}] \tag{46}$$

$$\begin{aligned}\mathbb{V}\text{ar}[Y_{k_l,m}] =& \mathbb{E}[\zeta_m]^2\mathbb{V}\text{ar}[\xi_{k_l,m}] + \mathbb{E}[\xi_{k_l,m}]^2\mathbb{V}\text{ar}[\zeta_m] \\ &+ \mathbb{V}\text{ar}[\zeta_m]\mathbb{V}\text{ar}[\xi_{k_l,m}],\end{aligned} \tag{47}$$

Therefore, $\mathbb{E}\left[Y_{k_l,m}\right]$ and $\mathbb{V}\text{ar}\left[Y_{k_l,m}\right]$ can be evaluated by substituting (42), (43), (44) and (45), into (46) and (47). Further, $\mathbb{E}[Y_{k_l}] = M\mathbb{E}\left[Y_{k_l,m}\right]$ and $\mathbb{V}\text{ar}[Y_{k_l}] = M\mathbb{V}\text{ar}\left[Y_{k_l,m}\right]$. Hence, the mean and variance of Y_{k_l} can be given as follows

$$\mathbb{E}[Y_{k_l}] = \frac{M\pi L_{\frac{1}{2}}(-\kappa_h)L_{\frac{1}{2}}(-\kappa_g)}{4\sqrt{(\kappa_h+1)(\kappa_g+1)}}, \tag{48}$$

$$\mathbb{V}\text{ar}[Y_{k_l}] = M - \frac{M\pi^2 L_{\frac{1}{2}}(-\kappa_h)^2 L_{\frac{1}{2}}(-\kappa_g)^2}{16(\kappa_h+1)(\kappa_g+1)}, \tag{49}$$

and by matching the mean and variance of Y_{k_l} in (48) and (49), with the $k\theta$ mean and $k\theta^2$ variance of the Gamma distribution, Y_{k_l} can be approximated as $Y_{k_l} \sim \Gamma(k_{Y_{k_l}}, \theta_{Y_{k_l}})$ with the shape $k_{Y_{k_l}}$ and scale $\theta_{Y_{k_l}}$ parameters:

$$k_{Y_{k_l}} = \frac{\mathbb{E}[Y_{k_l}]^2}{\mathbb{V}\text{ar}[Y_{k_l}]} \quad and \quad \theta_{Y_{k_l}} = \frac{\mathbb{V}\text{ar}[Y_{k_l}]}{\mathbb{E}[Y_{k_l}]}, \tag{50}$$

Accordingly, the n^{th} moment of Y_{k_l} can be given as

$$\mathbb{E}[Y_l^n] = \frac{\Gamma(k_{Y_{k_l}}+n)}{\Gamma(k_{Y_{k_l}})}\theta_{Y_{k_l}}^n, \tag{51}$$

since we are interested to approximate $Y_{k_l}^2$, we need to evaluate its mean $\mathbb{E}[Y_{k_l}^2]$ and variance $\mathbb{V}\text{ar}[Y_{k_l}^2]$. Hence, the first two moments of $Y_{k_l}^2$ can be calculated from the moments of Y_{k_l} by setting $n=2$ and $n=4$ in (51), respectively:

$$\mathbb{E}[Y_{k_l}^2] = \frac{\Gamma(k_{Y_{k_l}}+2)}{\Gamma(k_{Y_{k_l}})}\theta_{Y_{k_l}}^2, \tag{52}$$

$$\mathbb{V}\text{ar}[Y_{k_l}^2] = \frac{\Gamma(k_{Y_{k_l}}+4)}{\Gamma(k_{Y_{k_l}})}\theta_{Y_{k_l}}^4 - \left(\frac{\Gamma(k_{Y_{k_l}}+2)}{\Gamma(k_{Y_{k_l}})}\theta_{Y_{k_l}}^2\right)^2. \tag{53}$$

Now $Y_{k_l}^2$ can be approximated as $Y_{k_l}^2 \sim \Gamma(k_{Y_{k_l}^2}, \theta_{Y_{k_l}^2})$ with $k_{Y_{k_l}^2}$ and $\theta_{Y_{k_l}^2}$ given as follows:

$$k_{Y_{k_l}^2} = \frac{\mathbb{E}[Y_{k_l}^2]^2}{\mathbb{V}\text{ar}[Y_{k_l}^2]} \quad and \quad \theta_{Y_{k_l}^2} = \frac{\mathbb{V}\text{ar}[Y_{k_l}^2]}{\mathbb{E}[Y_{k_l}^2]}, \tag{54}$$

and by scaling with $\alpha_{k_l}\rho_{k_l}$, γ_{k_l} can be approximated as $\gamma_{k_l} \sim \Gamma(k_{Y_{k_l}^2}, \alpha_{k_l}\rho_{k_l}\theta_{Y_{k_l}^2})$, and hence, we obtain the CDF in (11). Further, the PDF of (12) can be obtained from [46, Eq. (3.3.6)], while the MGF can be given by [40], and the proof is completed.

APPENDIX B

IMPACT OF SECTORIZATION ON SPECTRAL EFFICIENCY

In order to glean more insights and to demonstrate the effect of increasing the number of sectors on the received power, let us express the spectral efficiency in terms of the mean and variance of Y_{k_l}, by utilizing the following relation

$$\mathbb{E}[Y_{k_l}^2] = \mathbb{E}[Y_{k_l}]^2 + \mathbb{V}\text{ar}[Y_{k_l}], \tag{55}$$

hence, by substituting (20) and (21) into (55), the spectrum efficiency in (24) can be rewritten as follows

$$\mathcal{R} = \frac{1}{K}\sum_{l=1}^{L}\sum_{k=1}^{K_l}\log_2\left(1+\rho_{k_l}\alpha_{k_l}\left[M^2\Omega + M(1-\Omega)\right]\right), \tag{56}$$

where $\Omega = \frac{\pi^2 L_{\frac{1}{2}}(-\kappa_h)^2 L_{\frac{1}{2}}(-\kappa_g)^2}{16(\kappa_h+1)(\kappa_g+1)}$. By assuming the total number of configurable elements of the whole BD-RIS is $Z=LM$, (56) can be further expressed as

$$\mathcal{R} = \frac{1}{K}\sum_{l=1}^{L}\sum_{k=1}^{K_l}\log_2\left(1+A\left[\frac{\frac{Z^2}{L^2}\Omega + \frac{Z}{L}(1-\Omega)}{\left(1-\cos\frac{\pi}{L}\right)^2}\right]\right), \tag{57}$$

where $A = \frac{\rho_{k_l}\lambda^4 G_t G_r}{4^3\pi^4 d_a^{\eta_a} d_b^{\eta_b}}$. Note that, $\cos\frac{\pi}{L} \in [0,1]$, for $L \in \{2,3,...,6\}$. For instance, when the total number of configurable elements Z are distributed into $L=2$ and $L=6$ sectors, we have the expressions in (25) and (26), respectively. With that, the proof is complete.

REFERENCES

[1] M. Samy, A. B. M. Adam, K. Ntontin, H. AI-Hraishawi, , S. Chatzinotas, and B. Otteresten, "Enhancing spectral and energy efficiency with multi-sector beyond-diagonal RIS," in *IEEE 25th Int. Workshop on Signal Process. Adv. Wireless Commun.*, Lucca, Italy, Sep. 2024, pp. 1–6.

[2] Q. Wu and R. Zhang, "Towards smart and reconfigurable environment: Intelligent reflecting surface aided wireless network," *IEEE Commun. Mag.*, vol. 58, no. 1, pp. 106–112, Jan. 2020.

[3] E. Basar, M. Di Renzo, J. De Rosny, M. Debbah, M.-S. Alouini, and R. Zhang, "Wireless communications through reconfigurable intelligent surfaces," *IEEE Access*, vol. 7, pp. 116 753–116 773, Feb. 2019.

[4] S. Kisseleff, W. A. Martins, H. Al-Hraishawi, S. Chatzinotas, and B. Ottersten, "Reconfigurable intelligent surfaces for smart cities: Research challenges and opportunities," *IEEE Open J. Commun. Soc.*, vol. 1, pp. 1781–1797, Nov. 2020.

[5] M. Samy, H. Al-Hraishawi, S. Chatzinotas, and B. Otteresten, "Outage performance of multiple hybrid active relays and RISs-assisted NOMA networks," *IEEE Wireless Commun. Lett.*, vol. 13, no. 9, pp. 2322–2326, Sep. 2024.

[6] M. Di Renzo, K. Ntontin, J. Song, F. H. Danufane, X. Qian, F. Lazarakis, J. De Rosny, D.-T. Phan-Huy, O. Simeone, R. Zhang, M. Debbah, G. Lerosey, M. Fink, S. Tretyakov, and S. Shamai, "Reconfigurable intelligent surfaces vs. relaying: Differences, similarities, and performance comparison," *IEEE Open J. Commun. Soc.*, vol. 1, pp. 798–807, Jun. 2020.

[7] J. An, C. Xu, D. W. K. Ng, G. C. Alexandropoulos, C. Huang, C. Yuen, and L. Hanzo, "Stacked intelligent metasurfaces for efficient holographic mimo communications in 6g," *IEEE J. Sel. Areas Commun.*, vol. 41, no. 8, pp. 2380–2396, 2023.

[8] Y. Liu, X. Mu, J. Xu, R. Schober, Y. Hao, H. V. Poor, and L. Hanzo, "STAR: Simultaneous transmission and reflection for 360° coverage by intelligent surfaces," *IEEE Wireless Commun.*, vol. 28, no. 6, pp. 102–109, Dec. 2021.

[9] H. Li, S. Shen, and B. Clerckx, "Beyond diagonal reconfigurable intelligent surfaces: From transmitting and reflecting modes to single-, group-, and fully-connected architectures," *IEEE Trans. Wireless Commun.*, vol. 22, no. 4, pp. 2311–2324, Apr. 2023.

[10] S. Shen, B. Clerckx, and R. Murch, "Modeling and architecture design of reconfigurable intelligent surfaces using scattering parameter network analysis," *IEEE Trans. Wireless Commun.*, vol. 21, no. 2, pp. 1229–1243, Feb. 2022.

[11] Özlem Tuğfe Demir and E. Björnson, "Wideband channel capacity maximization with beyond diagonal ris reflection matrices," 2024.

[12] H. Li, M. Nerini, S. Shen, and B. Clerckx, "Wideband modeling and beamforming for beyond diagonal reconfigurable intelligent surfaces," *arXiv preprint arXiv:2403.12893*, 2024.

[13] T. Fang and Y. Mao, "A low-complexity beamforming design for beyond-diagonal RIS aided multi-user networks," *IEEE Commun. Lett.*, vol. 28, no. 1, pp. 203–207, Jan. 2024.

[14] A. S. de Sena, M. Rasti, N. H. Mahmood, and M. Latva-aho, "Beyond diagonal ris for multi-band multi-cell MIMO networks: A practical frequency-dependent model and performance analysis," *arXiv preprint arXiv:2401.06475*, 2024.

[15] T. Esmaeilbeig, K. V. Mishra, and M. Soltanalian, "Beyond diagonal RIS: Key to next-generation integrated sensing and communications?" *arXiv preprint arXiv:2402.14157*, 2024.

[16] M. Nerini, S. Shen, and B. Clerckx, "Closed-form global optimization of beyond diagonal reconfigurable intelligent surfaces," *IEEE Trans. Wireless Commun.*, vol. 23, no. 2, pp. 1037–1051, Feb. 2024.

[17] ——, "Discrete-value group and fully connected architectures for beyond diagonal reconfigurable intelligent surfaces," *IEEE Trans. Veh. Technol.*, Dec. 2023.

[18] T. D. Hua, M. Mohammadi, H. Q. Ngo, and M. Matthaiou, "Cell-free massive MIMO SWIPT with beyond diagonal reconfigurable intelligent surfaces," *arXiv preprint arXiv:2402.00646*, 2024.

[19] M. Soleymani, I. Santamaria, A. Sezgin, and E. Jorswieck, "Maximizing spectral and energy efficiency in multi-user MIMO OFDM systems with RIS and hardware impairment," *arXiv preprint arXiv:2401.11921*, 2024.

[20] M. Nerini, G. Ghiaasi, and B. Clerckx, "Localized and distributed beyond diagonal reconfigurable intelligent surfaces with lossy interconnections: Modeling and optimization," *arXiv preprint arXiv:2402.05881*, 2024.

[21] A. Mahmood, T. X. Vu, W. U. Khan, S. Chatzinotas, and B. Ottersten, "Joint computation and communication resource optimization for beyond diagonal UAV-IRS empowered MEC networks," *arXiv preprint arXiv:2311.07199*, 2023.

[22] B. Wang, H. Li, S. Shen, Z. Cheng, and B. Clerckx, "A dual-function radar-communication system empowered by beyond diagonal reconfigurable intelligent surface," *arXiv preprint arXiv:2301.03286*, 2023.

[23] M. Nerini, S. Shen, and B. Clerckx, "Static grouping strategy design for beyond diagonal reconfigurable intelligent surfaces," 2024.

[24] H. Li, S. Shen, and B. Clerckx, "A dynamic grouping strategy for beyond diagonal reconfigurable intelligent surfaces with hybrid transmitting and reflecting mode," *IEEE Trans. Veh. Technol.*, vol. 72, no. 12, pp. 16 748–16 753, Dec. 2023.

[25] M.-A. Kim, S.-G. Yoo, H.-D. Kim, K.-H. Shin, Y.-H. You, and H.-K. Song, "Group-connected impedance network of ris-assisted rate-splitting multiple access in mu-mimo wireless communication systems," *Sensors*, vol. 23, no. 8, p. 3934, 2023.

[26] H. Li, S. Shen, and B. Clerckx, "Beyond diagonal reconfigurable intelligent surfaces: A multi-sector mode enabling highly directional full-space wireless coverage," *IEEE J. Sel. Areas in Commun.*, vol. 41, no. 8, pp. 2446–2460, Aug. 2023.

[27] ——, "Synergizing beyond diagonal reconfigurable intelligent surface and rate-splitting multiple access," *IEEE Trans. Wireless Commun.*, 2024.

[28] Y. Dong, Q. Li, S. X. Ng, and M. El-Hajjar, "Reconfigurable intelligent surface relying on low-complexity joint sector non-diagonal structure," *IEEE Open J. Veh. Technol.*, vol. 5, pp. 1106–1123, 2024.

[29] Y. Zhang, X. Shao, H. Li, B. Clerckx, and R. Zhang, "Full-space wireless sensing enabled by multi-sector intelligent surfaces," 2024. [Online]. Available: https://arxiv.org/abs/2406.15945

[30] H. Al-Hraishawi and G. Amarasuriya, "Sum rate analysis of cognitive massive MIMO systems with underlay spectrum sharing," in *IEEE Global Commun. Conf. GLOBECOM*, Washington, DC, USA, Dec. 2016, pp. 1–7.

[31] S. Atapattu, R. Fan, P. Dharmawansa, G. Wang, J. Evans, and T. A. Tsiftsis, "Reconfigurable intelligent surface assisted two-way communications: Performance analysis and optimization," *IEEE Trans. Commun.*, vol. 68, no. 10, pp. 6552–6567, Oct. 2020.

[32] J. Ye, A. Kammoun, and M.-S. Alouini, "Spatially-distributed RISs vs relay-assisted systems: A fair comparison," *IEEE Open J. Commun. Soc.*, vol. 2, pp. 799–817, Feb. 2021.

[33] W. Zhao, G. Wang, S. Atapattu, T. A. Tsiftsis, and C. Tellambura, "Is backscatter link stronger than direct link in reconfigurable intelligent surface-assisted system?" *IEEE Commun. Lett.*, vol. 24, no. 6, pp. 1342–1346, Jun. 2020.

[34] M. Samy, H. AI-Hraishawi, S. Kisseleff, S. Chatzinotas, and B. Otteresten, "Multiple RIS-assisted cooperative NOMA with user selection," in *IEEE Global Commun. Conf. GLOBECOM*, Kuala Lumpur, Malaysia, Dec. 2023, pp. 1405–1410.

[35] A. M. Salhab and M. H. Samuh, "Accurate performance analysis of reconfigurable intelligent surfaces over rician fading channels," *IEEE Wireless Commun. Lett.*, vol. 10, no. 5, pp. 1051–1055, Feb. 2021.

[36] X. Yue, J. Xie, Y. Liu, Z. Han, R. Liu, and Z. Ding, "Simultaneously transmitting and reflecting reconfigurable intelligent surface assisted NOMA networks," *IEEE Trans. Wireless Commun.*, vol. 22, no. 1, pp. 189–204, Jan. 2022.

[37] I. Gradshteyn, I. Ryzhik, and R. H. Romer, *Tables of integrals, series, and products*. American Association of Physics Teachers, 1988.

[38] M. Samy, H. Al-Hraishawi, K. Ntontin, S. Chatzinotas, and B. Otteresten, "RIS-empowered relays for cooperative NOMA," in *IEEE Wireless Commun. Net. Conf. (WCNC)*, Dubai, United Arab Emirates, Apr. 2024, pp. 1–6.

[39] Z. Wang and G. Giannakis, "A simple and general parameterization quantifying performance in fading channels," *IEEE Trans. Commun.*, vol. 51, no. 8, pp. 1389–1398, Aug. 2003.

[40] M. K. Simon and M. S. Alouini, *Digital Communication over Fading Channels*. New York, NY: John Wiley & Sons, 2000.

[41] W. R. Inc., "Mathematica online, Version 13.3," champaign, IL, 2023. [Online]. Available: https://functions.wolfram.com/HypergeometricFunctions/Hypergeometric2F1/03/01/

[42] C. Huang, A. Zappone, G. C. Alexandropoulos, M. Debbah, and C. Yuen, "Reconfigurable intelligent surfaces for energy efficiency in wireless communication," *IEEE Trans. Wireless Commun.*, vol. 18, no. 8, pp. 4157–4170, Aug. 2019.

[43] E. Björnson, Ö. Özdogan and E. G. Larsson, "Intelligent reflecting surface versus decode-and-forward: How large surfaces are needed to beat relaying?" *IEEE Wireless Commun. Lett.*, vol. 9, no. 2, pp. 244–248, Feb. 2020.

[44] M. Rao, F. J. Lopez-Martinez, M.-S. Alouini, and A. Goldsmith, "MGF approach to the analysis of generalized two-ray fading models," *IEEE Trans. Wireless Commun.*, vol. 14, no. 5, pp. 2548–2561, May 2015.

[45] W. R. Inc., "Mathematica online, Version 13.3," champaign, IL, 2023. [Online]. Available: https://functions.wolfram.com/Polynomials/LaguerreL/26/01/01/

[46] G. Casella and R. L. Berger, *Statistical Infence*, 2nd ed. Duxbury, 2002.